Stem Cell Reports
Article
OPEN ACCESS

# Human Neural Precursor Cells Promote Neurologic Recovery in a Viral Model of Multiple Sclerosis

Lu Chen,[1,7] Ronald Coleman,[2,7] Ronika Leang,[1] Ha Tran,[2] Alexandra Kopf,[1] Craig M. Walsh,[1] Ilse Sears-Kraxberger,[3] Oswald Steward,[4] Wendy B. Macklin,[5] Jeanne F. Loring,[2,*] and Thomas E. Lane[1,6,*]

[1]Department of Molecular Biology and Biochemistry, Sue and Bill Gross Stem Cell Center, Multiple Sclerosis Research Center, University of California, Irvine, Irvine, CA 92697, USA
[2]Center for Regenerative Medicine, Department of Chemical Physiology, The Scripps Research Institute, La Jolla, CA 92037, USA
[3]Reeve-Irvine Research Center, University of California, Irvine, Irvine, CA 92697, USA
[4]Reeve-Irvine Research Center, Departments of Anatomy & Neurobiology, Neurobiology & Behavior, and Neurosurgery, School of Medicine, University of California, Irvine, Irvine, CA 92697, USA
[5]Department of Cell and Developmental Biology, School of Medicine, University of Colorado, Aurora, CO 80045, USA
[6]Present address: Division of Microbiology & Immunology, Department of Pathology, School of Medicine, University of Utah, Salt Lake City, UT 84112, USA
[7]Co-first author
*Correspondence: jloring@scripps.edu (J.F.L.), tom.lane@path.utah.edu (T.E.L.)
http://dx.doi.org/10.1016/j.stemcr.2014.04.005


## SUMMARY

Using a viral model of the demyelinating disease multiple sclerosis (MS), we show that intraspinal transplantation of human embryonic stem cell-derived neural precursor cells (hNPCs) results in sustained clinical recovery, although hNPCs were not detectable beyond day 8 posttransplantation. Improved motor skills were associated with a reduction in neuroinflammation, decreased demyelination, and enhanced remyelination. Evidence indicates that the reduced neuroinflammation is correlated with an increased number of $CD4^+CD25^+FOXP3^+$ regulatory T cells (Tregs) within the spinal cords. Coculture of hNPCs with activated T cells resulted in reduced T cell proliferation and increased Treg numbers. The hNPCs acted, in part, through secretion of TGF-β1 and TGF-β2. These findings indicate that the transient presence of hNPCs transplanted in an animal model of MS has powerful immunomodulatory effects and mediates recovery. Further investigation of the restorative effects of hNPC transplantation may aid in the development of clinically relevant MS treatments.

## INTRODUCTION

Multiple sclerosis (MS) is a chronic inflammatory disease of the central nervous system (CNS) involving immune cell infiltration into the central nervous system (CNS), which results in demyelination and axonal loss that culminates in extensive neurological disability (Steinman, 1996). The demyelination is progressive over time; however, spontaneous, but transient, myelin repair can occur during the course of the disease. Endogenous oligodendrocyte precursor cells (OPCs) are believed to be responsible for spontaneous remyelination (Lassmann et al., 1997), but it is unclear why these cells only act intermittently. An important unmet clinical need for MS patients is an effective method to induce sustained remyelination.

Cell transplantation therapy is a promising approach to promote remyelination in MS patients; human embryonic stem cells (hESCs) and induced pluripotent stem cells, as well as fetal brain, are potential sources of therapeutic cells (Brüstle et al., 1999; Müller et al., 2006). Studies in animal models have demonstrated the benefits of cell therapy in treating mouse models of MS. For example, myelin generation (Buchet et al., 2011), accompanied by modulation of inflammatory responses, followed CNS transplantation of human neural precursor cells into animal models in which myelin formation is defective or demyelination is induced via immunization with encephalitogenic peptides. Another model, which we employed in this study, is based on findings that persistent infection with a mouse neurotropic coronavirus correlates with chronic neuroinflammation and immune-mediated demyelination (Lane and Buchmeier, 1997).

Here, we demonstrate sustained neurologic recovery out to 6 months following intraspinal transplantation of hESC-derived NPCs (hNPCs) into mice in which inflammatory-mediated demyelination was initiated by persistent viral infection of the CNS. We observed clinical recovery associated with muted neuroinflammation and decreased demyelination, along with emergence of $CD4^+CD25^+FOXP3^+$ regulatory T cells (Tregs). Ablation of Tregs in hNPC-transplanted mice inhibited the improvement in motor skills and increased neuroinflammation and in vitro, hNPCs modulated cytokine secretion and proliferation by antigen-sensitized T cells. Interestingly, the hNPCs were rapidly rejected after transplantation into these immunocompetent mice, indicating that the sustained neurologic recovery was not dependent on stable engraftment of hNPCs.

## RESULTS

### Intraspinal Injection of Human ESC-Derived Neural Precursor Cells Results in Clinical Improvement of JHMV-Infected Mice

Human neural precursor cells (hNPCs) were derived from WA09 hESCs using modifications of published protocols (Trosset et al., 2006; Vogt et al., 2011). An important modification was cell passaging to control cell density during the 9-day-directed differentiation protocol, and the transplanted cells had a uniform cellular morphology (Figure 1A). Because there is considerable phenotypic diversity among preparations of neural precursor cells (Müller et al., 2008), we performed extensive microarray-based transcriptome analysis to define a genomic phenotype for the cells that showed clinical activity. The microarray analysis revealed a consistent profile of gene expression among separate populations of hNPCs differentiated by our method (Figure 1B; Table S1 available online).

To evaluate the effects of hNPCs in promoting clinical recovery, we injected cells into the spinal cords of immunocompetent mice with established JHMV-induced clinical disease (Carbajal et al., 2010), which was generated by the injection of susceptible mice with the neurotropic JHM strain of mouse hepatitis virus (JHMV); consistent with previous studies, the mice showed viral persistence in white matter tracts and hind-limb paralysis, as well as demyelination and neuroinflammation (Templeton and Perlman, 2007).

Injection of hESC-derived hNPCs, but not human fibroblasts, resulted in a reduction in the severity of clinical disease and improved motor skills (Figure 1C) that were sustained out to 6 months posttransplantation (pt) (Figure 1D). Of 96 mice injected with hNPCs, 66 (73%) displayed a significant ($p < 0.05$) improvement in motor skill recovery, whereas nine of the 63 mice (14%) transplanted with the vehicle control improved. Living cells and intraspinal injection were necessary for the clinical recovery; transplantation of dead cells or delivery of cells via intravenous or intraperitoneal injection did not result in improved clinical outcome (data not shown).

Because transplantation of the hNPCs was performed in immunocompetent mice, we expected the cells to be rapidly rejected. To track the fate of the cells following injection, we transplanted hNPCs constitutively expressing the *Photinus pyralis* luciferase gene and monitored their presence by daily luciferin injection and IVIS imaging. Luciferase signals within the spinal cord were highest at day 1 pt and declined below the level of detection by day 8 pt. (Figure 1E). Imaging of transplanted cells revealed that the hNPCs did not migrate extensively within the spinal cord and did not disseminate into peripheral tissues. To confirm the imaging data, spinal cords from hNPC-transplanted mice were removed at defined times pt, serially sectioned 5 mm rostral and 5 mm caudal to the injection site, and immunostained for a human-specific cytoplasmic antigen (Uchida et al., 2012). As shown in Figure 1F, hNPCs were detected at days 1 and 4 pt, but staining was very weak by day 7 pt. These findings confirm that transplanted hNPCs survived for approximately 1 week after transplantation.

### Neuroinflammation and Demyelination Was Reduced in hNPC-Transplanted Mice

To investigate potential mechanisms underlying hNPC-mediated improvement in neurologic function, we examined neuroinflammation in hNPC-transplanted mice. Analysis of spinal cords from hNPC-transplanted mice at 21 days pt revealed a marked reduction in inflammatory cells present within spinal cords compared to the controls. Clinical recovery following hNPC transplantation is associated with reduced neuroinflammation in the spinal cord (Figure 2A). Immunostaining for activated macrophage/microglia and T cells (Figures 2B and 2C), critical in amplifying the severity of demyelination in JHMV-infected mice, revealed an overall reduction in immunoreactive cells within the spinal cords that was sustained past 175 days pt. (data not shown). Quantification of macrophage/microglia and T cell immunostaining indicated that hNPC transplantation resulted in a significant ($p < 0.01$) reduction in both cell populations compared to control mice (Figure 2D). Flow cytometry analysis confirmed immunostaining by showing reduced infiltration of $CD4^+$ and $CD8^+$ T cells into the CNS of hNPC-treated mice compared to controls (Figures 3A and 3B). Accumulation of virus-specific $CD4^+$ and $CD8^+$ T cells in the CNS of hNPC-treated mice was also determined by tetramer staining (Zhao et al., 2011). Infiltration of $CD4^+$ T cells recognizing the immunodominant epitope within the viral matrix (M) glycoprotein spanning amino acids 133–147 (M133–147) and $CD8^+$ T cells specific for the immunodominant epitope in the spike glycoprotein located on amino acids 510–518 (S510–518) were both reduced in hNPC-transplanted mice (Figures 3A and 3B). In addition, macrophage ($F4/80^+CD45^{high}$) infiltration was reduced in hNPC-transplanted mice (Figure 3C). Analysis of viral titers within the CNS of experimental mice indicated that control of viral replication within the spinal cords was not affected by hNPC transplantation; replicating virus was not detected (Figure 3D), and there were no differences in transcript levels of viral RNA (Figure 3E).

Spinal cord sections from transplanted mice that displayed improved motor function showed a dramatic reduction in the severity of demyelination when compared to control mice (Figure 4A). Quantification of demyelination indicated a significant ($p < 0.05$) reduction in white

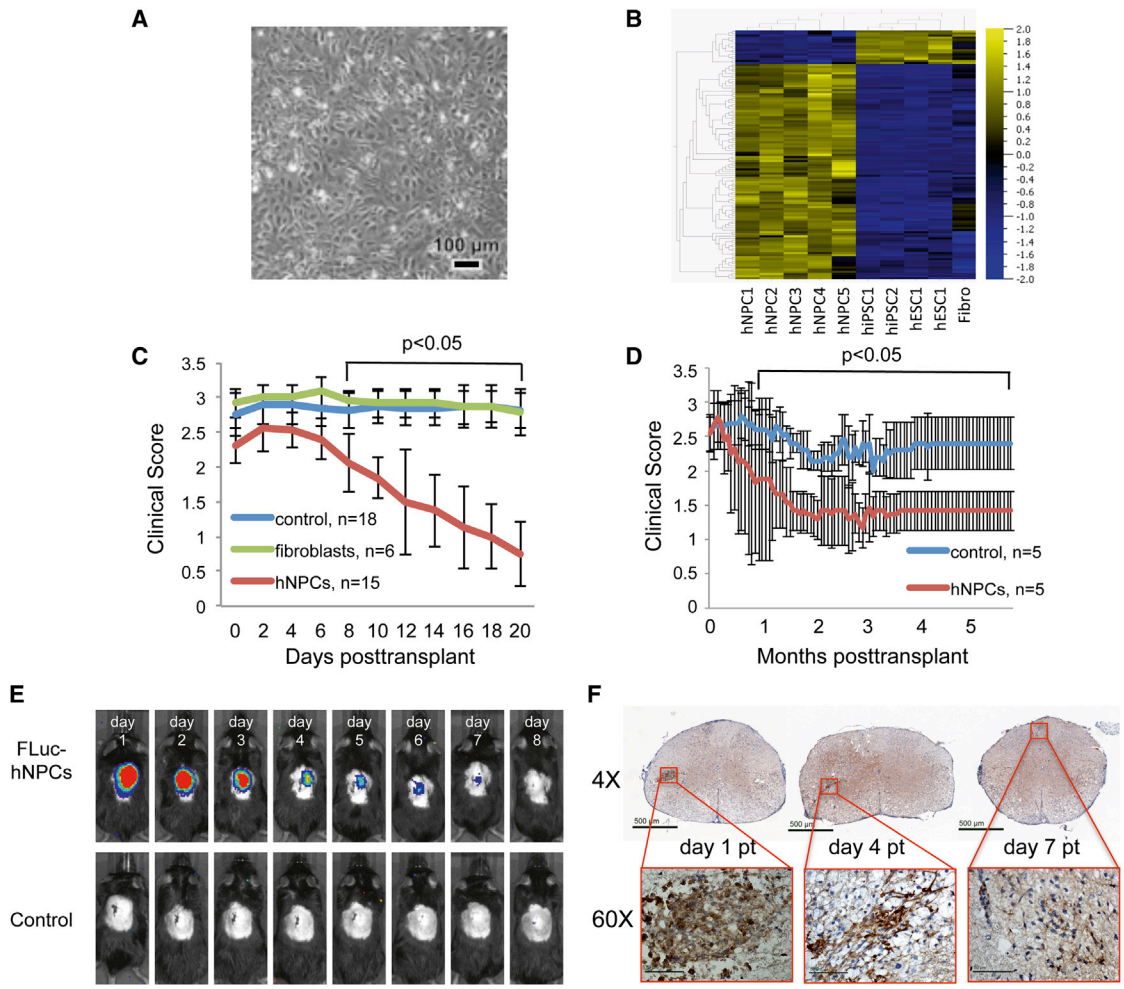


**Figure 1. Characteristics and Transplantation of hESC-Derived NPCs into JHMV-Infected Mice**

(A) Human neural precursor cells (hNPCs) after 9 days of directed differentiation. The cells are closely packed and have a distinctive morphology, and the culture appears to be homogeneous.

(B) Gene expression signature of hNPCs used for transplantation experiments. A heatmap shows the hierarchical clustering of 118 probes that were significantly differentially expressed ($p < 0.001$) in hNPCs. Five independent cultures of hNPCs were compared by global gene expression analysis (Human HT-12 v. 4 Expression Beadchip), with four samples of human pluripotent stem cells (two hESC and two iPSC lines) and a sample of human fibroblasts. The scale at right indicates the fold differences in gene expression, with yellow indicating relatively higher expression and blue indicating relatively lower expression.

(C) Human fibroblasts or hNPCs were transplanted by intraspinal injection into JHMV-infected mice at day 14 postinfection. hNPC-transplanted mice improved ($p < 0.05$) motor skills compared to animals transplanted with either fibroblasts or vehicle alone (control).

(D) Improved ($p < 0.05$) clinical recovery in hNPC-transplanted JHMV-infected mice was sustained out to 168 days posttransplantation (pt) when compared to infected mice treated with vehicle alone. For experiments shown in (C) and (D), the data are the results of two independent experiments with data shown as averages ± SEM.

(E) Daily IVIS imaging of luciferase-labeled hNPCs revealed that following intraspinal transplantation, cells were reduced to below the level of detection by day 8 posttransplantation; representative mice are shown. IVIS imaging was performed on vehicle-transplanted mice as a control.

(F) Representative immunohistochemical staining for human cells (STEM121 antibody) at defined times pt confirms IVIS imaging data and shows that following intraspinal transplantation, hNPCs are gradually eliminated, with very few cells remaining by day 7 post-transplant; 60× images are of framed areas in the 4× images.

matter damage in mice treated with hNPCs (1.9 ± 0.4, n = 9) compared to control mice (3.1 ± 0.1, n = 7) (Figure 4B). EM analysis of spinal cord sections was performed to determine whether remyelination was occurring in hNPC-transplanted mice. Assessment of the g-ratio, the ratio of the inner axonal diameter to the total outer fiber

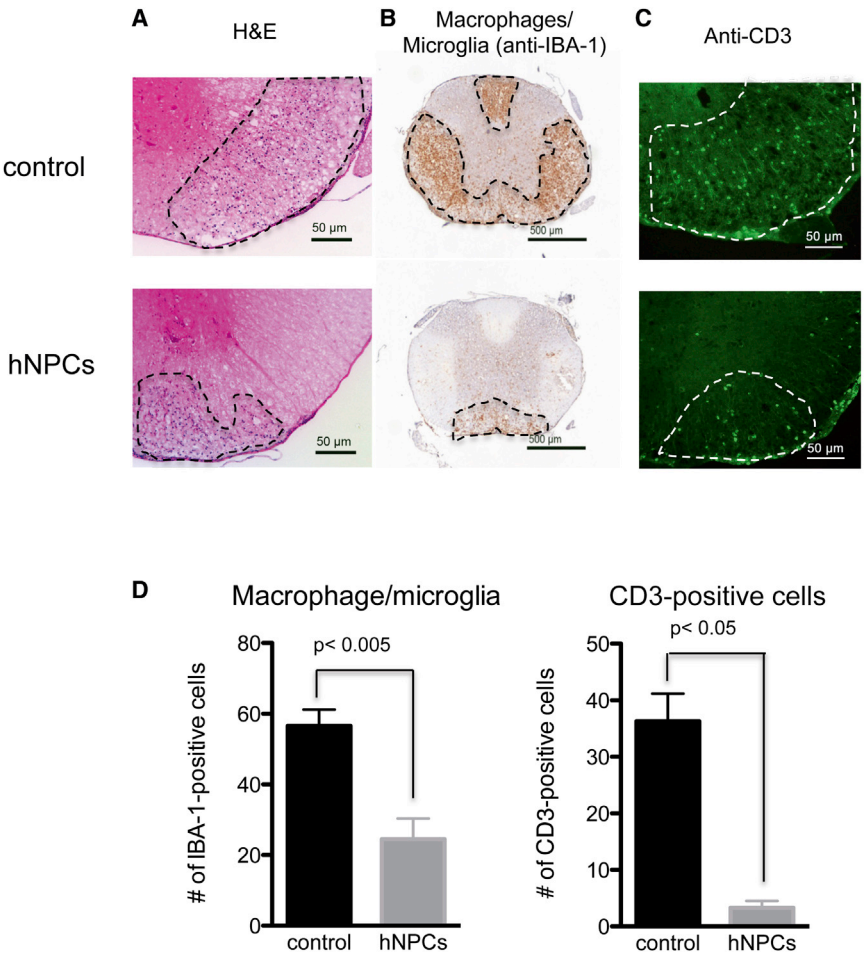


**Figure 2. hNPC-Mediated Clinical Recovery Is Associated with Dampened Neuroinflammation at Day 21 Pt**

(A) Clinical recovery following hNPC transplantation was associated with reduced neuroinflammation indicated by H&E staining of spinal cord sections (upper panel, control; lower panel, hNPC-treated). (B and C) Immunohistochemical staining demonstrated reduced (B; upper panel, control; lower panel, hNPC-treated) macrophage infiltration/microglia activation (IBA-1 reactivity, brown) and (C) CD3-positive lymphocytes (pan-T cell marker, Alexa 488/green staining) within spinal cords of hNPC-treated and control mice (upper panel, control; lower panel, hNPC-treated). (D) Quantification of IBA-1 and CD3-reactive cells indicated a significant reduction in macrophage/microglia and CD3-positive cells following hNPC transplantation compared to control mice. Data are representative of at least two independent experiments with a minimum of three mice per group; data are presented as averages ± SEM. Mann-Whitney t tests were used to determine the p values.

diameter, is a structural index of remyelination; lower ratios indicate more extensive myelination (Liu et al., 2001; Moore et al., 2013). The calculated g-ratio of hNPC-transplanted mice (0.83 ± 0.005, n = 533 axons) was significantly ($p < 0.001$) lower than that of control mice (0.94 ± 0.005, n = 541 axons) at 3 weeks pt (Figure 4C), indicating a greater degree of myelination in the transplanted mice.

### hNPC Treatment Increased the Frequency of $CD4^+CD25^+FOXP3^+$ Treg Cells within the CNS

Tregs have been shown to dampen neuroinflammation within the CNS of JHMV-infected mice (Trandem et al., 2010). In our studies, hNPC-mediated clinical recovery was associated with muted CNS inflammation, suggesting that the transplanted hNPCs may have promoted recovery through Treg-mediated mechanisms. Flow analysis of dissociated cells from spinal cords revealed an increased frequency of Tregs ($CD4^+CD25^+FOXP3^+$) in the spinal cords of hNPC-transplanted mice at day 10 pt (Figures 5A and 5B). In order to clarify the role of Tregs in improved clinical recovery, hNPCs transplanted mice were treated at days −2, 0, and +2 pt with anti-CD25 monoclonal antibody, which efficiently blocks Treg activity (Kohm et al., 2006). Flow analysis of $CD4^+CD25^+FOXP3^+$ T cells within draining cervical lymph nodes of anti-CD25-treated mice at day 9 pt confirmed efficient depletion of Tregs (>95%) (data not shown). This treatment inhibited functional improvement in hNPC-transplanted mice out to day 20 pt (Figure 5C). Further, the anti-CD25 treatment was associated with increased neuroinflammation in hNPC-transplanted animals when compared to transplanted animals treated with control antibody (Figures 5D and 5E).

We determined whether hNPCs influenced cytokine expression and proliferation of activated T cells; previous studies reported that transplanted hNPCs could modulate T-cell-mediated cytokine secretion (Liu et al., 2013), and secretion of proinflammatory cytokines, including IFN-γ and TNF-α, has been suggested to contribute to the severity of demyelination (Pewe and Perlman, 2002; Sun et al., 1995). Stimulation of T cells isolated from hNPC-transplanted mice with virus-specific $CD4^+$ peptide resulted in reduced ($p < 0.05$) expression of proinflammatory cytokines IFN-γ and TNF-α, whereas expression of

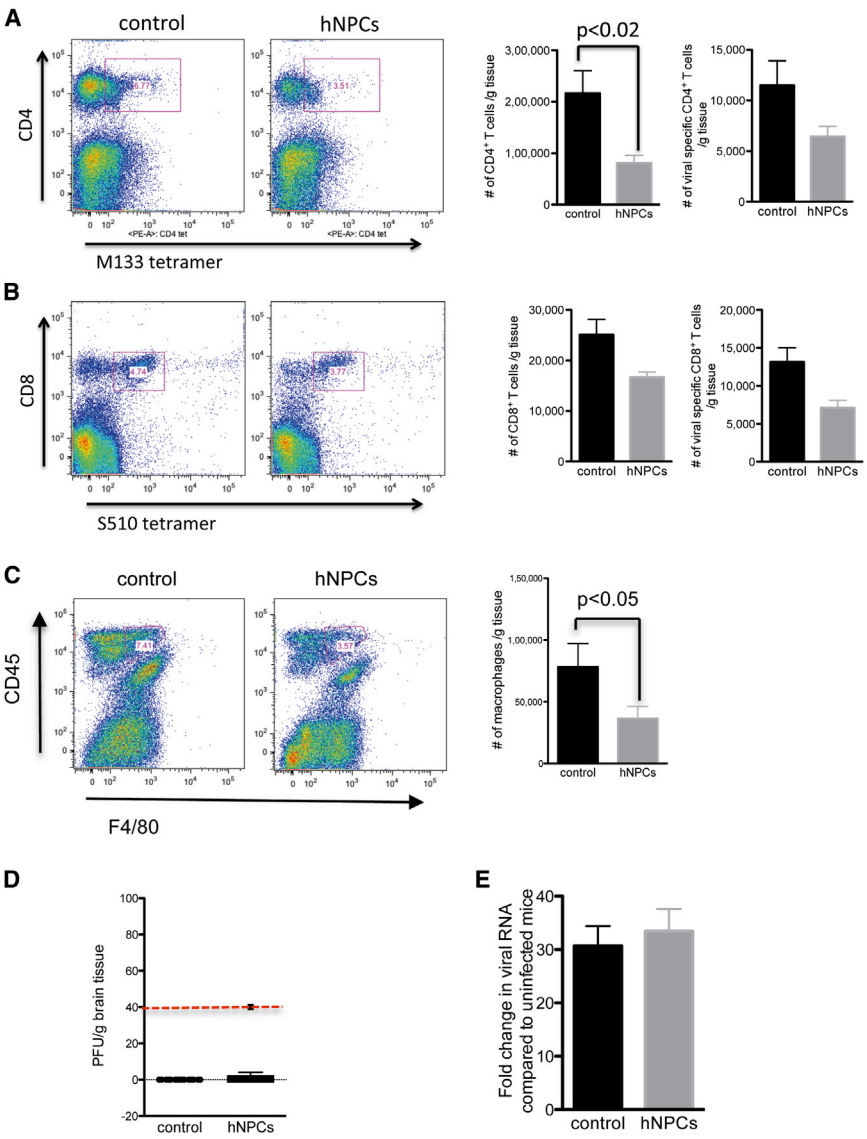


**Figure 3. hNPC Transplantation Restricts T Cell and Macrophage Infiltration into the CNS**

(A–C) Spinal cords from hNPC-treated and control mice were removed at 3 weeks pt, and infiltrating cells were immunophenotyped by flow staining for defined surface antigens (A) Infiltration of total $CD4^+$ T cells and virus-specific $CD4^+$ cells was reduced in hNPC-treated mice compared to controls. In addition, infiltration of $CD8^+$ cells and virus-specific $CD8^+$ T cells (B) was also reduced in hNPC-transplanted animals compared to controls. (C) Macrophage ($F4/80^+CD45^{high}$) accumulation in spinal cords was reduced in hNPC-transplanted mice compared to control mice. Representative flow dot blots are shown in (A), (B), and (C). Bar graphs are representative of at least two independent experiments with a minimum of four mice per experimental group; data are presented as averages ± SEM. Paired t tests were used to determine the p values.

(D and E) hNPC-mediated clinical recovery was not associated with increased spinal cord viral burden as determined by plaque assay (D) and quantitative PCR analysis of viral RNA (E). For results in (D) and (E), data are representative of at least two independent experiments with a minimum of three mice per experimental group. Data in (E) represent averages ± SEM. Mann-Whitney t tests were used to determine the p values.

anti-inflammatory IL-10 was elevated ($p < 0.001$) compared to control mice (Figure 6A). We determined whether the hNPC-induced protective effect was mediated by suppression of virus-specific T cell proliferation, as this could contribute to clinical recovery. Coculture of hNPCs with splenocytes obtained from JHMV-immunized mice and pulsed with the $CD4^+$ T-cell-specific immunodominant epitope M133–147 peptide resulted in a dose-dependent suppression of proliferation of $CD4^+$ T cells (Figure 6B) that was associated with an increased frequency of $CD4^+CD25^+FOXP3^+$ T cells (Figure 6C). Further characterization revealed that proliferation of virus-specific M133–147 $CD4^+$ T cells (Figure 6D), but not virus-specific S510–518 $CD8^+$ T cells (Figure 6E), was lower ($p < 0.001$) when compared to control cultures in which hNPCs were not included.

## TGF-β Signaling Was Required for the Anti-inflammatory Effect of Transplanted hNPCs

Our transplantation results indicated that the short-term presence of transplanted hNPCs resulted in long-term clinical recovery and decreased neuroinflammation and demyelination. This suggests that transplanted hNPCs may secrete factors that have long-term effects on neuroinflammation and demyelination. Recent studies have shown that certain hNPCs secrete the immunomodulatory cytokines TGF-β1 and TGF-β2 and there is an increase in the frequency of $CD4^+CD25^+FOXP3^+$ T cells following coculture of hNPCs with human PBMCs (Liu et al., 2013). Our microarray gene expression analysis identified TGF-β2 among the genes that were consistently more highly expressed in hNPCs compared to other cell types (Table S1). We used qRT-PCR to compare transcript levels in hESCs and hNPCs

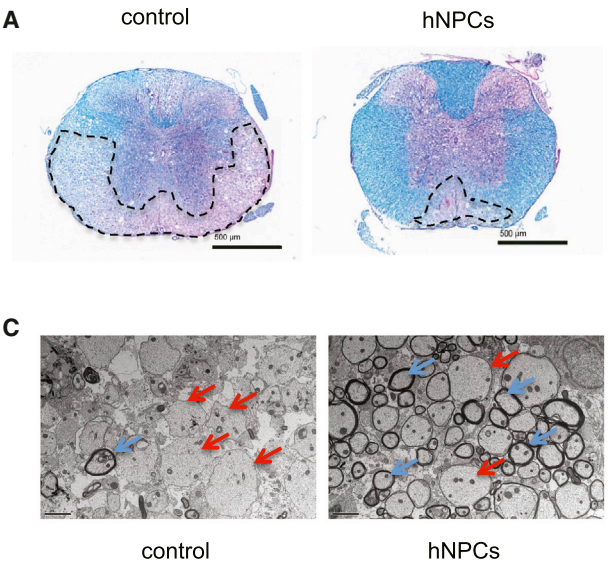


**Figure 4. hNPC Treatment Reduced the Severity of Demyelination**

(A) Representative luxol fast blue stain of spinal cord sections obtained from either hNPC-treated or control mice at 3 weeks pt. Dashed lines indicate areas of white matter damage.

(B) Quantification of the severity of demyelination at 3 weeks posttransplant indicates that white matter damage is significantly decreased ($p < 0.05$) in hNPC-treated versus control.

(C) Representative EM images (1200×) showing increased numbers of remyelinated axons (red arrows) compared to demyelinated axons (blue arrows) in hNPC-transplanted mice compared to control mice. Calculation of g-ratio, as a measurement of structural and functional axonal remyelination, revealed a significantly ($p < 0.001$) lower g-ratio (indicative of remyelination) in hNPC-treated mice (0.83 ± 0.005, n = 533 axons) compared to control mice (0.94 ± 0.005, n = 541 axons) at 3 weeks pt. For graphs shown in (B) and (C), data are representative of at least two independent experiments with a minimum of three mice per group; data are presented as average ± SEM; the Mann-Whitney t test was used to determine the p values.

and found that the TGF-β family of cytokines was differentially expressed ($p < 1 \times 10^{-6}$) in the hNPCs (Figure 7A). TGF-β2 transcripts were 250-fold higher in hNPCs, whereas TGF-β1 transcripts were ~5-fold higher compared to hESCs (Figure 7A). Hepatocyte growth factor (HGF) was previously shown to be associated with mesenchymal stem cell-mediated recovery in an experimental autoimmune encephalomyelitis (EAE) mouse model (Bai et al., 2012), but our results showed that HGF transcripts were nearly undetectable in our hNPCs (Figure 7A). Consistent with the transcript analysis, measurement of protein levels in culture medium conditioned by hNPCs showed that there was an approximate 40-fold higher level of TGF-β2 and a 3-fold higher level of TGF-β1 in hNPC-conditioned medium (CM) compared to control medium (Figure 7B). Inclusion of neutralizing antibodies specific for TGF-β1 or TGF-β2 blocked the ability of hNPCs to inhibit proliferation of virus-specific $CD4^+$ T cells, and inclusion of both antibodies had the largest effect (Figure 7C). In addition, antibody targeting of TGF-β1 or TGF-β2, alone or in combination, reduced numbers of $CD4^+CD25^+FOXP3^+$ T cells emerging in cocultures of hNPCs and T cells (Figure 7D), suggesting an important role for these cytokines in contributing to the immunomodulatory effects of hNPCs.

## DISCUSSION

There has been growing interest in the use of cell transplantation as therapy for neurological diseases since the first human trials using fetal neural precursors for Parkinson's disease were performed more than 20 years ago (reviewed in Barker et al., 2013). Currently, there are preclinical studies and clinical trials using fibroblastic adult mesenchymal stem cells (reviewed in Neirinckx et al., 2013) and fetal-derived neural cells (Uchida et al., 2012) for transplantation to treat neurological disease. A recent clinical study showed that fetal neural cell transplants promoted myelination in individuals afflicted with Pelizaeus-Merzbacher disease (PMD), a rare hypomyelinating disease (Gupta et al., 2012).

Multiple sclerosis (MS) is a demyelinating disease that is an attractive target for cell therapy because of the lack of long-term therapeutic benefit from current treatments. We investigated a cell-therapy strategy using human neural precursor cells derived from hESCs for their therapeutic potential in a mouse model of demyelination induced by viral infection. Available evidence indicates that the cause of MS is multifactorial and includes genetic background and environmental influences (Goodin, 2012; Pugliatti et al., 2008). Although no clear causal relationship between MS and viral infection has been firmly established, viruses are capable of persisting within the CNS and have been implicated in initiating or exacerbating MS symptoms (Gazouli et al., 2008).

We found that hNPC-mediated recovery in our model was associated with a marked reduction in neuroinflammation, characterized by reduced infiltration of inflammatory T cells and macrophages within the spinal cords and emergence of regulatory T cells (Tregs). Importantly, recovery

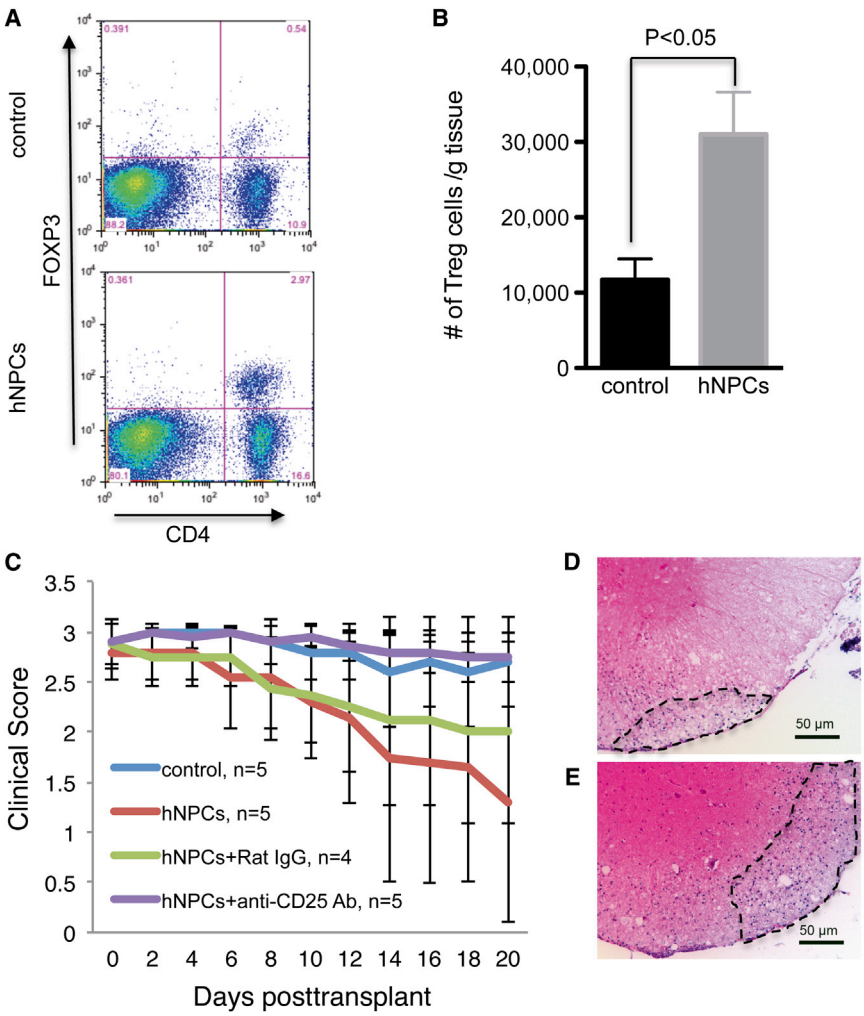


**Figure 5. hNPC-Mediated Recovery Is Associated with Treg Emergence within the Spinal Cord**

(A–E) Mice were infected intracranially with JMHV and transplanted with either hNPCs or vehicle alone at day 14 post-infection.(A) Examination of Tregs within the spinal cords by flow analysis ($CD4^+CD25^+FOXP3^+$) revealed an increased frequency of Tregs in hNPC-transplanted animals at day 10 post-transplantation, a time at which animals began to display improved motor skills compared to control mice. A representative flow cytometric dot blot is shown. (B) Quantification of Treg numbers in spinal cords of mice indicated a significant ($p < 0.05$) increase in the number of Tregs in hNPC-transplanted mice versus controls from 8–10 days posttransplantation. Data are representative of three independent experiments with a minimum of three mice per group; data are presented as average ± SEM. Mann-Whitney t tests were used to determine the p values. (C) hNPC-transplanted mice receiving anti-CD25 antibody did not display recovery in motor skills as compared to hNPC-treated mice treated with control antibody. (D and E) H&E staining of spinal cords of hNPC-treated mice treated with either control antibody (D) or anti-CD25 (E) indicates that depletion of Tregs increases neuroinflammation within white matter tracts (representative images are shown).

occurred in spite of the rapid rejection of the hNPCs in these immunocompetent mice. In MS, as in other neurodegenerative diseases, there is growing evidence that long-term survival of transplanted cells is not required for beneficial effects. A recent study (Bai et al., 2012) reported that mesenchymal stem-cell-induced recovery in the EAE mouse model and in lysolecithin-induced demyelination was dependent upon release of HGF. Although we have found that our hNPCs do not produce detectable HGF mRNA or protein, our findings are similar with regard to immunomodulation, diminished spread of demyelination, and remyelination. Additional studies also support the immunomodulatory properties associated with transplanted stem cells; in one study, intracerebroventricularly injected human glial cells rapidly died yet resulted in reduction of the clinical severity of EAE that correlated with inhibited proliferation of myelin-specific T cells (Kim et al., 2012b). Similarly, human ESC-derived oligodendrocyte precursors did not survive past 8 days following intraventricular injection into mice with EAE, yet animals displayed decreased neurologic disability, and this was associated with increased numbers of regulatory T cells within the CNS (Kim et al., 2012a). These reports are consistent with growing evidence that transplanted stem cells rarely differentiate into cells of neural lineage, and their efficacy often appears to be through delivery of trophic factors (Blurton-Jones et al., 2009; Müller et al., 2006) or by modulating inflammation (Neirinckx et al., 2013).

An important question that remains an area of ongoing work is to determine whether the sustained presence of Tregs after hNPC rejection continues to dampen neuroinflammation long term. We believe this is possible because hNPCs had already disappeared from the spinal cord at the time we detected increased numbers of Tregs. Our results suggest that Tregs are a critical component of the recovery, because antibody-mediated ablation of Tregs reduced the clinical effects of hNPCs. We are interested in characterizing cytokine profiles within both the CNS and draining cervical lymph nodes, as recent studies argue that

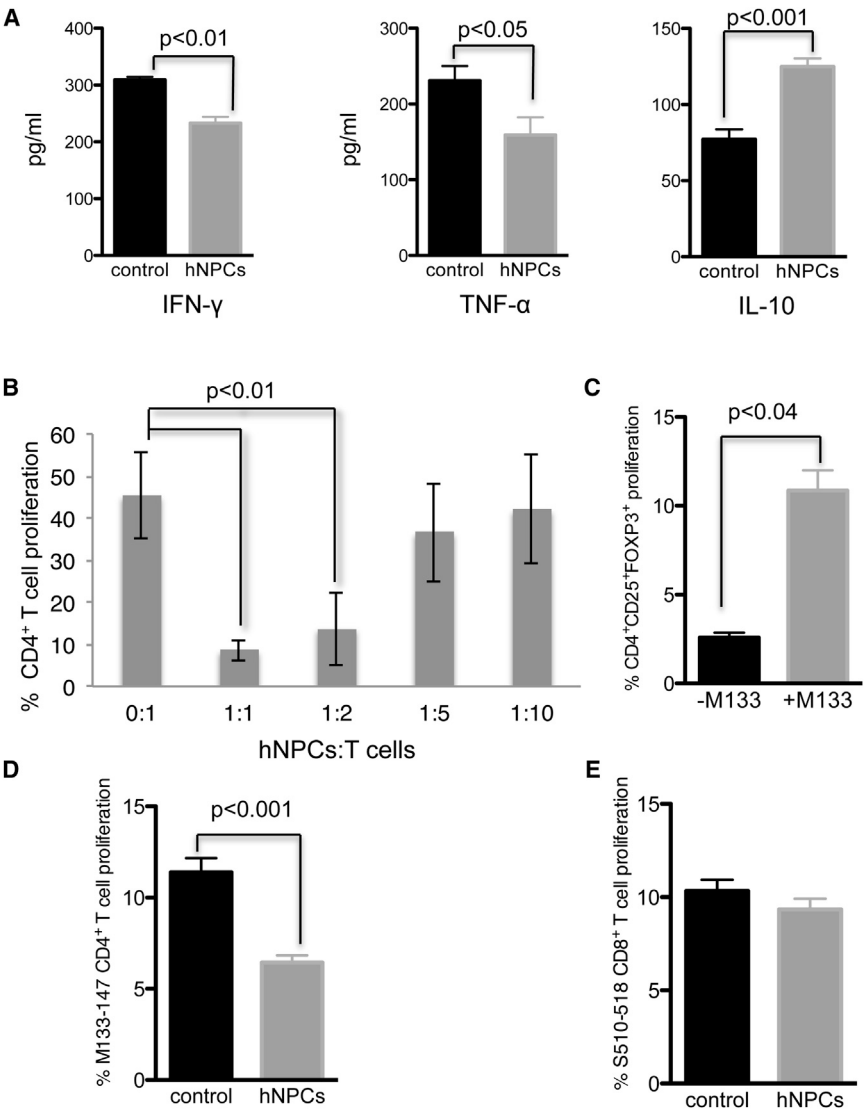


**Figure 6. hNPCs Modulate T Cell Responses**

(A) T cells were isolated from draining cervical lymph nodes of control and hNPC-transplanted mice at 3 weeks pt, stimulated with M133–144 viral peptide, and their secretion of IFN-γ, TNF-α, and IL-10 was determined by ELISA after 48 hr of culture. IFN-γ and TNF-α secretion was lower and IL-10 secretion higher in hNPC-treated mice.

(B) hNPCs were cocultured with activated T cells at the indicated ratios, and T cell proliferation was determined by eFluor 670 staining. Results demonstrated that hNPCs suppressed T cell proliferation in a dose-dependent manner.

(C) Coculture of hNPCs with activated T cells either in the presence or absence of the immunodominant CD4 viral peptide (M133–147) revealed increased numbers of $CD4^+$ $CD25^+FOXP3^+$ T cells when viral peptide was included.

(D) Coculture with hNPCs inhibited proliferation ($p < 0.001$) of M133–147 $CD4^+$ T cells.

(E) S510–518-specific $CD8^+$ T cells were not affected following coculture with hNPCs.

Data are representative of at least two independent experiments with a minimum of three mice per group; data are presented as average ± SEM. Mann-Whitney t tests were used to determine the p values in (A) and (B); paired t tests were used to determine the p values in (C) to (E).

Treg-mediated effects in controlling neuroinflammation and demyelination in JHMV-infected mice occurs in lymphatic tissue (Trandem et al., 2010) and that certain cytokines can function in controlling Treg suppression (Zhao et al., 2011). As it is unlikely that transplanted hNPCs were differentiating into oligodendroglia, it appears that remyelination is occurring in response to activation of endogenous OPCs through mechanisms that remain to be defined. One possible mechanism is that the transplanted cells or Tregs, or both, may secrete factors that influence maturation of OPCs.

Our studies suggest that direct delivery of precursor cells into the CNS via intraspinal transplantation influences clinical and histologic outcome through interactions of transplanted cells with inflammatory cells present within the CNS microenvironment, such as by affecting the emergence of Tregs. This suggests that transplanted hNPCs can manipulate the microenvironment, presumably through localized secretion of soluble factors that modulate the immune response and remyelination. Our work and the work of others (Liu et al., 2013) shows that cultured hNPCs secrete anti-inflammatory cytokines, including TGF-β1 and TGF-β2. Based on our experiments and previous reports, our current hypothesis is that the emergence of Tregs in the areas of the transplant may be due to localized expression of TGF-β1 and/or TGF-β2 following hNPC transplantation. The immunodulatory effects of TGF-β in regulating immune tolerance and T cell homeostasis are well documented (Sakaguchi, 2004), and our findings indicate an important role for TGF-β1 and TGF-β2 in contributing to the hNPC-mediated inhibition of proliferation of antigen-specific T cells and in increasing the frequency of regulatory T cells. This evidence supports the idea that the presence of transplanted hNPCs suppresses the

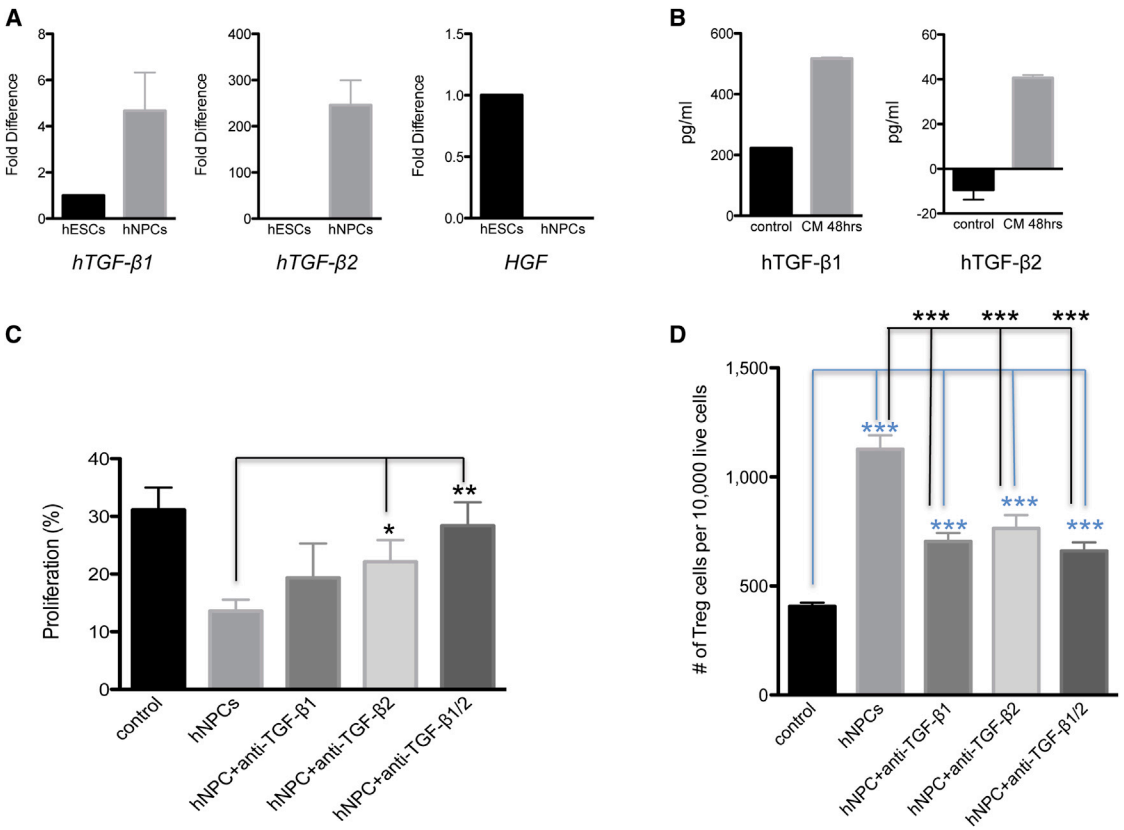


**Figure 7. TGF-β Secretion and T Cell Responses**

(A) RNA was extracted from hNPCs at day 9 of neural differentiation, and qRT-PCR was used to determine relative transcript levels of *TGF-β1*, *TGF-β2*, and *HGF*. Values were normalized to internal GAPDH levels and are shown as fold differences compared to undifferentiated hESC expression levels using ΔΔCt calculations; data are presented as averages ± SEM.

(B) ELISA determination of TGF-β1 and TGF-β2 in culture medium conditioned by hNPCs compared to unconditioned medium; data are presented as average ± SEM and representative of three independent experiments.

(C) In hNPC-T cell cocultures, inclusion of anti-TGF-β1 or anti-TGF-β2 alone or in combination impaired the ability of hNPCs to block proliferation of virus-specific $CD4^+$ T cells.

(D) Antibody targeting of TGF-β1 or TGF-β2 reduced the numbers of $CD4^+CD25^+$ $FOXP3^+$ Tregs. (C) and (D) contain data of a minimum of four mice per group; mean values are presented; error bars represent SEM. Mann-Whitney t tests were used to determine the p values in (A) and (B); paired t tests were used to determine the p values for (C) and (D); * $p < 0.05$, ** $p < 0.01$, *** $p < 0.001$.

proliferation of virus-specific T cells, reducing production of proinflammatory cytokines IFN-γ and TNF-α, while enhancing the increase in T regulatory cells that coincides with clinical recovery.

In summary, we demonstrate that transplantation of hNPCs into a mouse model of viral-induced demyelination results in prolonged clinical recovery up to at least 6 months in spite of the disappearance of transplanted hNPCs after only a week. Importantly, we found that the methods used to prepare the hNPCs are critical to their functional phenotype. Human neural precursor cells are notably diverse (Müller et al., 2008), and culture methods (Chetty et al., 2013; Nazareth et al., 2013) have profound effects on cellular differentiation. To facilitate further investigation of the cells and the mechanisms underlying hNPC-mediated recovery, we generated a genomic phenotype of the cells that can serve as a guide to define the precise cell type used in our studies.

Our findings extend the existing evidence that long-term engraftment is not important for sustained clinical and histologic recovery. Our evidence points to secreted factors produced by the hNPCs in the local environment as the regulators of T cell fate and remyelination activity by endogenous OPCs. Because they are produced by the hNPCs used in our study and have known effects on T cell development, members of the TGF-β family are strong candidates as triggers initiating clinical recovery. Our further studies will focus on identification and

validation of the secreted factors that are likely to underlie the restorative effects of transplanted hNPCs, which may guide further development of stem cell and perhaps cell-free therapies for MS.

## EXPERIMENTAL PROCEDURES

### Animals and Virus

Age-matched (5–7 weeks) C57BL/6 (H-$2^b$, National Cancer Institute [NCI]) were infected intracranially (ic) with 150 plaque-forming units (pfu) of MHV strain J2.2v-1 (JHMV) in 30 μl sterile Hank's balanced salt solution (Carbajal et al., 2010). Mice were sacrificed at various time points following hNPC transplantation, and tissues were removed and processed for analysis. All experiments were approved by the University of California, Irvine Institutional Animal Care and Use Committee protocols #1998-2022 and 2010-2943. Determination of viral titers from the CNS of infected mice was performed by isolating tissues at defined times after infection, homogenizing tissue, and overlaying clarified supernatant on the DBT astrocytoma cell line as previously described (Liu et al., 2001). For methods describing quantification of viral RNA in CNS tissues, please see the Supplemental Experimental Procedures.

### Generation of hNPCs

Feeder-free-adapted WA09 hESCs were seeded at a concentration of $1.0 \times 10^4$ cells per $cm^2$ in BD Matrigel Basement Membrane Matrix (BD Bioscience) on coated six-well plates and cultured for 24 hr in human embryonic stem cell culture medium (STEMPRO hESC SFM; Life Technologies). The medium was then replaced with NPC differentiation medium (Dulbecco's modified Eagle's medium [DMEM]/F12, 20% Knockout Serum Replacement [KSR] [Life Technologies], 1× nonessential amino acids [NEAA; Life Technologies], 1× GlutaMAX [Life Technologies], and 0.1 mM 2-mercaptoethanol [Life Technologies]) supplemented with 20 ng/ml of midkine (MK; Millipore), and small molecules: 2 μM each of dorsomorphin (6-[4-(2-Piperidin-1-ylethoxy) phenyl]-3-pyridin-4-ylpyrazolo [1,5-a] pyrimidine; Sigma), A 83-01 (3-(6-Methyl-2-pyridinyl)-*N*-phenyl-4-(4-quinolinyl)-1*H*-pyrazole-1-carbothioamide; Tocris), and PNU-74654 (benzoic acid, 2-phenoxy-, 2-[(5-methyl-2-furanyl)methylene] hydrazide; Sigma). Medium was changed daily. The cells were split 1:3 on days 3 and 6 using Accutase (Life Technologies). hNPCs were harvested for transplantation 9 days after the start of the differentiation protocol. For methods describing gene expression arrays and generation of LUC+ cells, please see the Supplemental Experimental Procedures.

### hNPC Transplantation

For transplantation studies, JHMV-infected mice received an injection of either $2.5 \times 10^5$ hNPCs or human fibroblasts (suspended in 2.5 μl DMEM/F12) at T9 of the spinal cord on day 14 pi. Control animals infected with virus were transplanted with DMEM/F12 alone at T9 of the spinal cord. For further details, refer to Carbajal et al. (2011).

### IVIS Imaging

Bioluminescence imaging (BLI) of firefly luciferase (FLUC)-expressing hNPCs was performed daily posttransplantation for 8 days, at which point no bioluminescent signal was observed. Mice were anesthetized by isofluorine gas inhalation via nose-comb and remained under sedation during imaging. Ten minutes prior to image acquisition, mice were injected intraperitoneally with 250 mg/kg body weight of D-luciferin in PBS. Photons emitted from transplanted cells were used to construct a pseudocolor image of bioluminescent intensity that was overlaid onto a gray-scale photograph of the mice.

### Histopathology and Immunohistochemistry

Animals were sacrificed by inhalation of an overdose of isoflurane (Western Medical Supplies) and perfused with PBS by cardiac perfusion. The spinal cords were harvested and fixed in 4% paraformaldehyde overnight before being embedded in resin or in OCT medium for cryosectioning as previously described (Totoiu et al., 2004). Cryosections of spinal cords were stained with Harrison hematoxylin and eosin (H&E) to visualize cellular inflammation or with luxol fast blue (LFB) and counterstained with H&E to assess the severity of demyelination. Scoring of resin-embedded sections was performed using a previously described method (Glass et al., 2004; Lane et al., 2000). In brief, the demyelination scale is as follows: 0, no demyelination; 1, mild inflammation accompanied by loss of myelin integrity; 2, moderate inflammation with increasing myelin damage; 3, numerous inflammatory lesions accompanied by significant increase in myelin stripping; and 4, intense areas of inflammation accompanied by numerous phagocytic cells engulfing myelin debris. All slides were blinded and read independently by two investigators. For immunohistochemical staining, cryosections (8 μm) were incubated at 4°C overnight with combinations of the following primary antibodies: STEM121 antibody (1:200 dilution; Stemcells) for detection of human NPCs, anti-iBA-1 antibody (1:400 dilution; Wako) for detection of activated macrophages/microglia, and anti-CD3 (1:200 dilution; BD PharMingen) as a pan-T cell marker. A biotinylated secondary antibody (1:400 dilution; Vector Laboratories) and the ABC Elite staining system (Vector Laboratories) were used to visualize the primary antibodies in accordance with the manufacturer's instructions. Diaminobenzidine (DAB) was used as a chromogen.

### Immunofluorescence

Cryosections (8 μm) were washed in PBS three times and then blocked with PBS with 0.03% Triton X-100 and 10% normal goat serum (NGS; Jackson ImmunoResearch) for 1 hr at room temperature. Rat anti-mouse CD3 and anti-mouse IBA-1 (1:400 dilution, Wako) (1:200 dilution; BD PharMingen) was applied to samples and incubated overnight at 4°C. Samples were washed again in PBS three times, and then Alexa-Fluor-conjugated secondary antibody (goat anti-rat Alexa 488; 1:500 in PBS; Invitrogen) was applied for 1 hr at room temperature. All slides were then washed in PBS and coverslip mounted using Vectashield Mounting Medium with DAPI (Vector Laboratories). Negative controls were incubated in PBS instead of primary antibodies. The number of immunopositive cells for anti-mouse CD3 and anti-IBA-1 staining was determined by using the ImageJ cell counter.

### Electron Microscopy and g-Ratio Analysis

For EM analysis of spinal cords, mice were sacrificed and underwent cardiac perfusion with 0.1 M cacodylate buffer containing 2% paraformaldehyde/2% glutaraldehyde. Serial ultrathin sections of spinal cords embedded in Epon epoxy resin were stained with uranyl acetate-lead citrate and analyzed as previously described (Liu et al., 2001). Images at 1,200× magnification were analyzed for g-ratio using ImageJ software. In adult animals there is a relationship between axon circumference and myelin sheath thickness (number of lamellae) expressed by the g-ratio (axon diameter/total fiber diameter); in remyelination, this relationship changes such that myelin sheaths are abnormally thin for the axons they surround. An abnormally thin myelin sheath, relative to axonal diameter, was used as the criterion for oligodendrocyte remyelination. Absence of a myelin sheath was used as the criterion for demyelination. For most axons, two measurements were conducted with a minimum of 500 axons analyzed per experimental group. In all cases, slides were blinded and read independently by three investigators.

### Isolation of Lymphocytes from Spinal Cord

Cells were isolated from the spinal cords of experimental mice as previously described (Lane et al., 2000). Single-cell suspensions were centrifuged for 30 min at 1,200 × g at 4°C over a discontinuous Percoll gradient and then Percoll and lipid layers were removed. Isolated cells were filtered, washed with 20 ml DMEM, centrifuged at 1,000 × g at 4°C, counted, and prepared for flow cytometry (see below). Cells isolated from spleens were used as positive controls.

### Flow Cytometry

Lymphocytes isolated from the spinal cord were immunophenotyped with fluorescent antibodies (1:200) for the following cell-surface markers: fluorescein isothiocyanate (FITC)-conjugated CD4 (GK1.5; BD Biosciences), PE-Cy7-conjugated CD8 (Ly-2; BD Biosciences), antigen-presenting cell (APC)-conjugated CD25 (PC61; BD Biosciences), APC-conjugated CD45 (30-F11; eBioscience), FITC-conjugated F4/80 (Ci-A3-1; Serotech), and Alexa Fluor 647-conjugated FOXP3 (FJK-16 s; eBioscience). PE-conjugated I-Ab/M133–147 tetramers and PE-conjugated $D^b$/S510–518 (8 μg/ml; obtained from the National Institutes of Health/National Institute of Allergy and Infectious Diseases MHC Tetramer Core Facility) were used to stain viral-specific CD4 T cells and viral-specific CD8 T cells, respectively. Appropriate isotype controls were used for each antibody. Cells were run on a LSRII flow cytometer (BD Biosciences) and analyzed with FlowJo software (Tree Star). All cells for flow cytometry were blocked with anti-mouse CD16/32 (Mouse Fc Block; 1:200; BD Biosciences) for 20 min at 4°C.

### Treatment of Mice with CD25 Antibody

JHMV-infected mice were intraperitoneally (i.p.) treated with 150 μg of a blocking antibody specific for mouse CD25 (rat anti-mouse CD25, clone PC61.5) or control rat immunoglobulin G (Sigma) in 100 μl sterile saline at days −2, 0, and 2 posttransplantation. Spinal cords were removed from hNPC-transplanted and control mice at day 10 posttransplantation, and the presence of CD4+CD25+FoxP3+ cells (Tregs) was assayed by flow cytometry (see above). Draining cervical lymph nodes were analyzed 9 days after antibody administration to determine efficacy of anti-CD25 treatment.

### T Cell Proliferation Assays

Splenocytes were isolated from JHMV (DM strain)-infected mice and pulsed with the $CD4^+$ T-cell-specific immunodominant M133–147 peptide for 24 hr. T cells were purified from the treated splenocytes by using the Pan T Cell Isolation Kit II (Miltenyi Biotec) and labeled with eFluor 670 (eBiosciences). T cells ($1 \times 10^5$ cells/well) in 200 μl complete medium (RPMI-1640 [Life Technologies] supplemented with 1× GlutaMAX-1 [Life Technologies], 1× nonessential amino acids [Life Technologies], 100 U/ml penicillin [Life Technologies], 100 μg/ml streptomycin [Life Technologies], 1 mM sodium pyruvate [Life Technologies], 55 μM 2-mercaptomethanol [Life Technologies], and 10% fetal bovine serum [Atlanta Biologicals]) were plated in round-bottomed 96-well plates (Corning) and incubated at 37°C, 5% $CO_2$, for 4 days before being analyzed by flow cytometry. Concanavalin A (2.5 μm/ml, Sigma-Aldrich) was used as a T cell proliferation stimulant. For the TGF-β1 and TGF-β2 blocking experiments, anti-TGF-β1 antibody ab64715 (0.5 μg/ml, Abcam) and anti-TGF-β2 antibody ab10850 (0.1 μg/ml, Abcam) were also included in the cell-culture medium.

### ELISAs

Levels of mouse IFN-γ, TNF-α, and IL-10 from stimulated T cells isolated from draining cervical lymph nodes were determined by ELISA using specific Mouse DuoSet in accordance with the manufacturer's specifications (R&D Systems). Human hepatocyte growth factor (HGF), TGF-β1, and TGF-β2 production by cultured hESCs and hNPCs was determined using human Quantikine ELISA Kits from R&D Systems in accordance with the manufacturer's specifications.

### qRT-PCR

The QuantiTect Reverse-Transcription Kit (QIAGEN) was used to generate cDNAs from RNA collected from cell samples. TaqMan gene expression probes were obtained for *TGFB1*, *TGFB2*, and *HGF* from Life Technologies. qRT-PCR was performed on the cDNAs using the TaqMan gene expression master mix (Life Technologies) to quantify transcript levels in a BioRad C1000 thermal cycler (Bio-Rad). Values were normalized to internal GAPDH levels and shown as a fold change of ESC expression using ΔΔCt calculations.

## ACCESSION NUMBERS

The Gene Expression Omnibus accession number for the microarray data reported in this paper is GSE56187.

## SUPPLEMENTAL INFORMATION

Supplemental Information includes Supplemental Experimental Procedures and one table and can be found with this article online at http://dx.doi.org/10.1016/j.stemcr.2014.04.005.

## AUTHOR CONTRIBUTIONS

L.C and R.C. designed and performed experiments, interpreted results, and helped write the manuscript; R.L., H.T., and A.K. assisted in performing experiments; C.M.W. and W.B.M. provided key reagents and helped edit the manuscript; I.S.-K. and O.S. performed electron microscopic analysis; J.F.L. and T.E.L. funded the project, provided conceptual overview, designed and interpreted experimental results, and wrote the manuscript.

## ACKNOWLEDGMENTS

This work was funded by grants from the California Institute for Regenerative Medicine (CIRM) (RM1-01717 and CL1-00502 to J.F.L., and TR3-05603 to C.M.W. and J.F.L.) and the National Multiple Sclerosis Society (RG-4925) (to T.E.L.). L.C. was supported by a CIRM postdoctoral fellowship (TG2-01152) and R.C. is a recipient of a Ken and Karen Craven Graduate Fellowship. We are grateful to Duane Roth for his unwavering support of stem cell research, and we wish to dedicate this report to his memory.

Received: October 17, 2013
Revised: April 4, 2014
Accepted: April 7, 2014
Published: May 15, 2014

## REFERENCES

Bai, L., Lennon, D.P., Caplan, A.I., DeChant, A., Hecker, J., Kranso, J., Zaremba, A., and Miller, R.H. (2012). Hepatocyte growth factor mediates mesenchymal stem cell–induced recovery in multiple sclerosis models. Nat. Neurosci. *15*, 862–870.

Barker, R.A., Barrett, J., Mason, S.L., and Björklund, A. (2013). Fetal dopaminergic transplantation trials and the future of neural grafting in Parkinson's disease. Lancet Neurol. *12*, 84–91.

Blurton-Jones, M., Kitazawa, M., Martinez-Coria, H., Castello, N.A., Müller, F.J., Loring, J.F., Yamasaki, T.R., Poon, W.W., Green, K.N., and LaFerla, F.M. (2009). Neural stem cells improve cognition via BDNF in a transgenic model of Alzheimer disease. Proc. Natl. Acad. Sci. USA *106*, 13594–13599.

Brüstle, O., Jones, K.N., Learish, R.D., Karram, K., Choudhary, K., Wiestler, O.D., Duncan, I.D., and McKay, R.D. (1999). Embryonic stem cell-derived glial precursors: a source of myelinating transplants. Science *285*, 754–756.

Buchet, D., Garcia, C., Deboux, C., Nait-Oumesmar, B., and Baron-Van Evercooren, A. (2011). Human neural progenitors from different foetal forebrain regions remyelinate the adult mouse spinal cord. Brain *134*, 1168–1183.

Carbajal, K.S., Schaumburg, C., Strieter, R., Kane, J., and Lane, T.E. (2010). Migration of engrafted neural stem cells is mediated by CXCL12 signaling through CXCR4 in a viral model of multiple sclerosis. Proc. Natl. Acad. Sci. USA *107*, 11068–11073.

Carbajal, K.S., Weinger, J.G., Whitman, L.M., Schaumburg, C.S., and Lane, T.E. (2011). Surgical transplantation of mouse neural stem cells into the spinal cords of mice infected with neurotropic mouse hepatitis virus. J. Vis. Exp., e2834.

Chetty, S., Pagliuca, F.W., Honore, C., Kweudjeu, A., Rezania, A., and Melton, D.A. (2013). A simple tool to improve pluripotent stem cell differentiation. Nat. Methods *10*, 553–556.

Gazouli, M., Sechi, L., Paccagnini, D., Sotgiu, S., Arru, G., Nasioulas, G., and Vassilopoulos, D. (2008). NRAMP1 polymorphism and viral factors in Sardinian multiple sclerosis patients. Can. J. Neurol. Sci. *35*, 491–494.

Glass, W.G., Hickey, M.J., Hardison, J.L., Liu, M.T., Manning, J.E., and Lane, T.E. (2004). Antibody targeting of the CC chemokine ligand 5 results in diminished leukocyte infiltration into the central nervous system and reduced neurologic disease in a viral model of multiple sclerosis. J. Immunol. *172*, 4018–4025.

Goodin, D.S. (2012). The genetic and environmental bases of complex human-disease: extending the utility of twin-studies. PLoS ONE *7*, e47875.

Gupta, N., Henry, R.G., Strober, J., Kang, S.M., Lim, D.A., Bucci, M., Caverzasi, E., Gaetano, L., Mandelli, M.L., Ryan, T., et al. (2012). Neural stem cell engraftment and myelination in the human brain. Sci. Transl. Med. *4*, ra137.

Kim, H., Walczak, P., Kerr, C., Galpoththawela, C., Gilad, A.A., Muja, N., and Bulte, J.W. (2012a). Immunomodulation by transplanted human embryonic stem cell-derived oligodendroglial progenitors in experimental autoimmune encephalomyelitis. Stem Cells *30*, 2820–2829.

Kim, H., Walczak, P., Muja, N., Campanelli, J.T., and Bulte, J.W. (2012b). ICV-transplanted human glial precursor cells are short-lived yet exert immunomodulatory effects in mice with EAE. Glia *60*, 1117–1129.

Kohm, A.P., McMahon, J.S., Podojil, J.R., Begolka, W.S., DeGutes, M., Kasprowicz, D.J., Ziegler, S.F., and Miller, S.D. (2006). Cutting Edge: Anti-CD25 monoclonal antibody injection results in the functional inactivation, not depletion, of CD4+CD25+ T regulatory cells. J. Immunol. *176*, 3301–3305.

Lane, T.E., and Buchmeier, M.J. (1997). Murine coronavirus infection: a paradigm for virus-induced demyelinating disease. Trends Microbiol. *5*, 9–14.

Lane, T.E., Liu, M.T., Chen, B.P., Asensio, V.C., Samawi, R.M., Paoletti, A.D., Campbell, I.L., Kunkel, S.L., Fox, H.S., and Buchmeier, M.J. (2000). A central role for CD4(+) T cells and RANTES in virus-induced central nervous system inflammation and demyelination. J. Virol. *74*, 1415–1424.

Lassmann, H., Brück, W., Lucchinetti, C., and Rodriguez, M. (1997). Remyelination in multiple sclerosis. Mult. Scler. *3*, 133–136.

Liu, M.T., Keirstead, H.S., and Lane, T.E. (2001). Neutralization of the chemokine CXCL10 reduces inflammatory cell invasion and demyelination and improves neurological function in a viral model of multiple sclerosis. J. Immunol. *167*, 4091–4097.

Liu, J., Götherström, C., Forsberg, M., Samuelsson, E.B., Wu, J., Calzarossa, C., Hovatta, O., Sundström, E., and Åkesson, E. (2013). Human neural stem/progenitor cells derived from embryonic stem cells and fetal nervous system present differences in immunogenicity and immunomodulatory potentials in vitro. Stem Cell Res. (Amst.) *10*, 325–337.

Moore, S., Khalaj, A.J., Yoon, J., Patel, R., Hannsun, G., Yoo, T., Sasidhar, M., Martinez-Torres, L., Hayardeny, L., and Tiwari-Woodruff, S.K. (2013). Therapeutic laquinimod treatment decreases inflammation, initiates axon remyelination, and improves motor deficit in a mouse model of multiple sclerosis. Brain Behav *3*, 664–682.

Müller, F.J., Snyder, E.Y., and Loring, J.F. (2006). Gene therapy: can neural stem cells deliver? Nat. Rev. Neurosci. *7*, 75–84.

Müller, F.J., Laurent, L.C., Kostka, D., Ulitsky, I., Williams, R., Lu, C., Park, I.H., Rao, M.S., Shamir, R., Schwartz, P.H., et al. (2008). Regulatory networks define phenotypic classes of human stem cell lines. Nature *455*, 401–405.

Nazareth, E.J., Ostblom, J.E., Lücker, P.B., Shukla, S., Alvarez, M.M., Oh, S.K., Yin, T., and Zandstra, P.W. (2013). High-throughput fingerprinting of human pluripotent stem cell fate responses and lineage bias. Nat. Methods *10*, 1225–1231.

Neirinckx, V., Coste, C., Rogister, B., and Wislet-Gendebien, S. (2013). Concise review: adult mesenchymal stem cells, adult neural crest stem cells, and therapy of neurological pathologies: a state of play. Stem Cells Transl Med *2*, 284–296.

Pewe, L., and Perlman, S. (2002). Cutting edge: CD8 T cell-mediated demyelination is IFN-gamma dependent in mice infected with a neurotropic coronavirus. J. Immunol. *168*, 1547–1551.

Pugliatti, M., Harbo, H.F., Holmøy, T., Kampman, M.T., Myhr, K.M., Riise, T., and Wolfson, C. (2008). Environmental risk factors in multiple sclerosis. Acta Neurol. Scand. Suppl. *188*, 34–40.

Sakaguchi, S. (2004). Naturally arising CD4+ regulatory t cells for immunologic self-tolerance and negative control of immune responses. Annu. Rev. Immunol. *22*, 531–562.

Steinman, L. (1996). Multiple sclerosis: a coordinated immunological attack against myelin in the central nervous system. Cell *85*, 299–302.

Sun, N., Grzybicki, D., Castro, R.F., Murphy, S., and Perlman, S. (1995). Activation of astrocytes in the spinal cord of mice chronically infected with a neurotropic coronavirus. Virology *213*, 482–493.

Templeton, S.P., and Perlman, S. (2007). Pathogenesis of acute and chronic central nervous system infection with variants of mouse hepatitis virus, strain JHM. Immunol. Res. *39*, 160–172.

Totoiu, M.O., Nistor, G.I., Lane, T.E., and Keirstead, H.S. (2004). Remyelination, axonal sparing, and locomotor recovery following transplantation of glial-committed progenitor cells into the MHV model of multiple sclerosis. Exp. Neurol. *187*, 254–265.

Trandem, K., Anghelina, D., Zhao, J., and Perlman, S. (2010). Regulatory T cells inhibit T cell proliferation and decrease demyelination in mice chronically infected with a coronavirus. J. Immunol. *184*, 4391–4400.

Trosset, J.Y., Dalvit, C., Knapp, S., Fasolini, M., Veronesi, M., Mantegani, S., Gianellini, L.M., Catana, C., Sundström, M., Stouten, P.F., and Moll, J.K. (2006). Inhibition of protein-protein interactions: the discovery of druglike beta-catenin inhibitors by combining virtual and biophysical screening. Proteins *64*, 60–67.

Uchida, N., Chen, K., Dohse, M., Hansen, K.D., Dean, J., Buser, J.R., Riddle, A., Beardsley, D.J., Wan, Y., Gong, X., et al. (2012). Human neural stem cells induce functional myelination in mice with severe dysmyelination. Sci. Transl. Med. *4*, ra136.

Vogt, J., Traynor, R., and Sapkota, G.P. (2011). The specificities of small molecule inhibitors of the TGFß and BMP pathways. Cell. Signal. *23*, 1831–1842.

Zhao, J., Zhao, J., Fett, C., Trandem, K., Fleming, E., and Perlman, S. (2011). IFN-γ- and IL-10-expressing virus epitope-specific Foxp3(+) T reg cells in the central nervous system during encephalomyelitis. J. Exp. Med. *208*, 1571–1577.

**Stem Cell Reports, Volume *2***

**Supplemental Information**

# Human Neural Precursor Cells Promote Neurologic Recovery in a Viral Model of Multiple Sclerosis

**Lu Chen, Ronald Coleman, Ronika Leang, Ha Tran, Alexandra Kopf, Craig M. Walsh, Ilse Sears-Kraxberger, Oswald Steward, Wendy B. Macklin, Jeanne F. Loring, and Thomas E. Lane**

## Supplemental Experimental Procedures

### Characterization of hNPCs by gene expression array

For hNPC samples and other control cell samples, one well of a 6-well plate containing approximately 10^6 cells was collected and pelleted by centrifugation. Each pellet was flash frozen and stored at -80$^{o}$C. RNA was purified using the mirVana miRNA Isolation Kit (Life Technologies). Collected RNA was quantified using the Qubit Fluorometer and RNA BR assay kit (Life Technologies). The RNA quality of each sample was determined using the 2100 Bioanalyzer (Agilent Technologies) to obtain an RNA integrity Number (RIN). Samples with acceptable RINs (8.2-10.0) were amplified, labeled and hybridized onto Illumina HumanHT-12 v4 Expression Beadchips according to the manufacturer's instructions. Hybridized chips were scanned using the iScan system (Illumina). Raw data extraction was performed with Genome Studio (Illumina) and probes without a detection p-value (a measure of confidence that the signal observed is above background fluorescence) of less than 0.01 in at least 1 sample were removed. The remaining probes were then quantile-normalized to correct for between-sample variation. Normalized data were then analyzed using Qlucore Omics Explorer (Qlucore).

### Generation of LUC$^{+}$ H9 cells

Stbl3 cells containing the plasmid pLenti CMV Puro LUC (w168-1) were obtained (Plasmid 17477; Addgene) and purified plasmid was transfected into a 6-well plate of confluent 293T cells for virus generation. The supernatant containing virus was collected 48 h post transfection and filtered through a 0.45μm filter. STEMPRO® hESC SFM

(Life Technologies) supplemented with 10µg/ml polybrene was added to a 6-well plate of feeder free adapted WA09 cells that were less than 50% confluent. 150µl of virus-containing supernatant per well was added and the plates were spinfected at 1800RPM for 1 hour at 37°C. After 48 hours, 5µg/ml puromycin was added to select for virally transduced cells. Medium was changed daily and puromycin selection was maintained. Firefly luciferase (FLUC) production was verified by adding luciferin to culture wells and imaging them using a Bio-Rad Gel Doc system (Bio-Rad).

**Viral RNA Quantification**

For quantitative RT-PCR experiments to determine viral RNA levels in spinal cords, primers specific for the JHMV spike protein (forward:GGCTGTTGACGCATGTGATT; reverse: GAGCACGCGTCTGAATGAAC) were designed using PrimerQuest software (Integrated DNA Technologies, Inc.). SYBR Green Real-Time PCR Master Mix (Life Technologies) was used according to manufacturer's specifications and RT-PCR was performed using the Applied Biosystems ViiA 7 Real-Time PCR System. $C_t$ values of S protein transcripts were normalized to β-actin $C_t$ values (forward: GGCCCAGAGCAAGAGAGGTATCC; reverse: ACGCACGATTTCCCTCTCAGC) and compared using the $\Delta\Delta C_t$ method.

**Table S1. Gene Expression Array Data from Figure 1B**

(Table begins on following page.)

| NAME | DESCRIPTION | NPC1 | NPC2 | NPC3 | NPC4 | NPC5 | iPSC1 | iPSC2 | ESC1 | ESC2 | Fibro |
|---|---|---|---|---|---|---|---|---|---|---|---|
| ILMN_1769694 | *ACCN2* | 1358.4 | 817.4 | 1531.3 | 1512.0 | 521.3 | 232.6 | 289.1 | 215.3 | 208.5 | 431.2 |
| ILMN_1658660 | *ACTC1* | 14512.5 | 20589.1 | 13632.2 | 18397.5 | 15337.5 | 692.4 | 794.8 | 775.4 | 747.3 | 1202.9 |
| ILMN_1713751 | *ADAM19* | 7057.0 | 10109.4 | 8829.5 | 10117.4 | 8227.5 | 1293.3 | 953.0 | 1250.7 | 1353.7 | 1019.3 |
| ILMN_1716264 | *ANKRD1* | 1297.4 | 1226.1 | 1808.1 | 921.1 | 1233.1 | 145.3 | 125.7 | 131.1 | 179.5 | 373.7 |
| ILMN_1678143 | *ARHGDIB* | 4263.2 | 5150.6 | 7285.0 | 8835.9 | 7360.0 | 193.7 | 168.6 | 190.6 | 175.8 | 671.3 |
| ILMN_1786041 | *ASB9* | 1309.6 | 882.2 | 544.6 | 1000.9 | 316.9 | 164.9 | 142.6 | 132.2 | 203.2 | 169.1 |
| ILMN_1752899 | *BCL11A* | 159.6 | 154.0 | 141.1 | 173.6 | 171.0 | 929.4 | 1052.4 | 1067.2 | 1940.4 | 291.7 |
| ILMN_2255133 | *BCL11A* | 119.3 | 130.4 | 111.3 | 113.1 | 166.6 | 936.0 | 1125.8 | 1062.1 | 1967.4 | 220.9 |
| ILMN_1740900 | *BMP4* | 5466.2 | 2667.2 | 6016.8 | 1994.9 | 1281.1 | 253.6 | 251.1 | 270.6 | 551.9 | 197.7 |
| ILMN_3239861 | *C10orf140* | 3941.0 | 3362.2 | 3217.2 | 2215.4 | 2086.7 | 865.4 | 695.7 | 516.9 | 709.1 | 331.3 |
| ILMN_1656369 | *C8orf4* | 624.7 | 931.3 | 526.7 | 693.0 | 2482.7 | 104.7 | 106.8 | 113.2 | 118.7 | 119.0 |
| ILMN_2195482 | *CACNB3* | 2381.5 | 2212.1 | 2836.3 | 2804.0 | 1972.1 | 402.0 | 647.1 | 362.1 | 617.7 | 1173.4 |
| ILMN_1719236 | *CDH5* | 808.3 | 914.5 | 1093.0 | 2974.0 | 2259.2 | 123.3 | 124.6 | 111.4 | 125.9 | 119.9 |
| ILMN_1731237 | *CLSTN2* | 713.4 | 1236.4 | 1371.9 | 1629.0 | 1636.0 | 127.0 | 120.6 | 124.6 | 142.6 | 131.0 |
| ILMN_1810054 | *CNN1* | 1723.1 | 2343.2 | 1023.6 | 2715.2 | 1637.4 | 273.8 | 294.9 | 219.5 | 214.8 | 324.8 |
| ILMN_1789507 | *COL11A1* | 3393.6 | 4130.0 | 4188.6 | 3354.4 | 1391.1 | 284.0 | 265.9 | 258.8 | 404.7 | 431.1 |
| ILMN_2392803 | *COL11A1* | 715.9 | 1098.8 | 680.0 | 971.6 | 617.4 | 166.8 | 148.0 | 146.3 | 177.4 | 179.1 |
| ILMN_1653028 | *COL4A1* | 13750.1 | 17375.0 | 14224.1 | 17508.3 | 19251.6 | 2446.1 | 3306.3 | 2672.5 | 3392.3 | 1799.8 |
| ILMN_1724994 | *COL4A2* | 1686.5 | 2072.7 | 1832.2 | 2722.0 | 1244.1 | 357.7 | 450.1 | 260.8 | 346.0 | 422.7 |
| ILMN_1809496 | *COPG2* | 261.4 | 287.6 | 278.2 | 209.1 | 188.6 | 1333.5 | 1246.3 | 1002.0 | 657.7 | 406.4 |
| ILMN_1784294 | *CPA4* | 675.6 | 781.9 | 1503.7 | 1420.7 | 2667.3 | 133.2 | 122.5 | 119.1 | 116.7 | 273.6 |
| ILMN_1731374 | *CPE* | 5804.3 | 7861.2 | 7046.8 | 6933.3 | 7280.0 | 554.1 | 598.6 | 486.3 | 455.6 | 959.3 |
| ILMN_1654072 | *CX3CL1* | 857.1 | 787.7 | 785.4 | 1036.0 | 349.2 | 174.1 | 243.3 | 199.3 | 219.4 | 117.0 |
| ILMN_1748323 | *CXCL14* | 931.6 | 1206.2 | 443.9 | 883.3 | 280.5 | 165.5 | 146.9 | 165.7 | 159.6 | 160.3 |
| ILMN_1758128 | *CYGB* | 775.4 | 713.8 | 824.8 | 1879.5 | 870.0 | 173.2 | 193.8 | 157.4 | 155.3 | 400.5 |
| ILMN_1807291 | *CYP1A1* | 219.2 | 505.0 | 503.9 | 1042.1 | 348.9 | 127.1 | 123.2 | 115.1 | 123.5 | 124.6 |
| ILMN_1741603 | *DBC1* | 141.1 | 161.0 | 146.6 | 200.5 | 168.3 | 1163.0 | 1184.5 | 1098.7 | 1418.0 | 559.1 |
| ILMN_1666503 | *DENND2A* | 2341.0 | 2600.8 | 2225.9 | 3975.8 | 1805.3 | 702.7 | 665.5 | 600.9 | 528.3 | 476.7 |
| ILMN_1682775 | *EDN1* | 2648.4 | 2435.0 | 1552.5 | 2855.5 | 3508.7 | 156.1 | 123.5 | 120.0 | 116.1 | 437.2 |
| ILMN_1796629 | *EDNRA* | 1475.2 | 1415.3 | 2101.6 | 848.4 | 1033.3 | 191.1 | 234.5 | 220.3 | 218.3 | 165.1 |
| ILMN_1703852 | *EFNB2* | 3049.8 | 5270.9 | 3514.2 | 3750.1 | 7589.1 | 880.1 | 688.9 | 453.3 | 1249.9 | 807.8 |
| ILMN_1779147 | *ENC1* | 1246.6 | 1384.7 | 1749.8 | 1453.9 | 2303.2 | 316.9 | 261.4 | 416.7 | 520.3 | 356.0 |
| ILMN_1668092 | *ESAM* | 368.8 | 1103.5 | 744.9 | 1272.5 | 807.4 | 132.6 | 120.0 | 121.6 | 138.4 | 114.8 |
| ILMN_2105919 | *FGF2* | 228.4 | 293.9 | 243.9 | 175.3 | 595.5 | 1390.6 | 1939.4 | 675.3 | 1501.1 | 2453.0 |
| ILMN_1665738 | *FLI1* | 521.6 | 538.9 | 576.1 | 902.2 | 859.3 | 131.2 | 134.4 | 143.7 | 143.6 | 331.2 |
| ILMN_1697491 | *FLJ14213* | 651.6 | 748.0 | 791.1 | 1069.9 | 1078.8 | 259.4 | 283.0 | 161.8 | 169.8 | 227.9 |
| ILMN_1805665 | *FLRT3* | 1367.0 | 1459.8 | 3317.6 | 756.4 | 1925.9 | 159.1 | 122.6 | 130.5 | 438.1 | 168.0 |
| ILMN_2406656 | *GATA3* | 472.8 | 427.5 | 875.0 | 556.0 | 355.0 | 114.5 | 125.7 | 120.9 | 160.8 | 133.0 |
| ILMN_1660549 | *GPR177* | 1489.8 | 1670.1 | 1795.2 | 963.2 | 753.7 | 136.6 | 154.8 | 144.5 | 186.0 | 341.2 |
| ILMN_1671260 | *GPR177* | 2753.1 | 2612.7 | 2836.6 | 1414.1 | 1251.2 | 167.0 | 137.3 | 167.6 | 230.2 | 443.9 |
| ILMN_1753913 | *GPR177* | 871.8 | 840.4 | 744.7 | 469.9 | 373.2 | 126.9 | 120.6 | 118.4 | 156.6 | 163.8 |
| ILMN_2283325 | *GPR177* | 8195.7 | 6197.0 | 6948.9 | 3702.4 | 3383.9 | 310.9 | 288.1 | 243.1 | 633.9 | 832.4 |
| ILMN_2399769 | *GPR177* | 1374.6 | 1677.3 | 1348.3 | 1003.2 | 856.7 | 153.9 | 136.9 | 135.3 | 221.6 | 268.4 |
| ILMN_2121408 | *HBEGF* | 1810.1 | 3336.5 | 2582.6 | 3729.9 | 5887.9 | 243.5 | 259.1 | 247.3 | 294.4 | 220.5 |

| | | | | | | | | | | | |
|---|---|---|---|---|---|---|---|---|---|---|---|
| ILMN_1653466 | *HES4* | 9815.7 | 13300.6 | 12883.0 | 12383.2 | 5076.5 | 502.4 | 961.3 | 510.4 | 821.5 | 536.1 |
| ILMN_1788203 | *HEY1* | 1128.3 | 984.6 | 1006.1 | 1577.7 | 1785.5 | 215.1 | 155.7 | 167.1 | 227.2 | 120.0 |
| ILMN_3236367 | *IFFO2* | 1126.1 | 942.1 | 1091.1 | 1598.3 | 1082.1 | 212.2 | 240.1 | 182.4 | 243.9 | 293.5 |
| ILMN_1778010 | *IL32* | 893.1 | 612.1 | 429.6 | 1332.9 | 605.4 | 128.4 | 122.1 | 129.3 | 118.8 | 152.3 |
| ILMN_2368530 | *IL32* | 1793.0 | 1168.8 | 1029.4 | 2640.2 | 1553.5 | 144.5 | 132.1 | 128.6 | 186.1 | 196.9 |
| ILMN_1685397 | *ITGA3* | 1565.2 | 1234.1 | 2656.8 | 3190.2 | 2023.0 | 423.2 | 414.2 | 373.5 | 452.9 | 550.0 |
| ILMN_1800697 | *LDB2* | 595.3 | 417.7 | 532.0 | 390.8 | 334.1 | 3864.7 | 2985.2 | 3052.1 | 4158.7 | 2191.4 |
| ILMN_2213136 | *LEF1* | 747.3 | 852.4 | 822.6 | 1013.4 | 647.5 | 155.0 | 146.2 | 117.7 | 186.5 | 129.6 |
| ILMN_1657373 | *LEPREL1* | 3482.0 | 5302.0 | 6330.5 | 4782.0 | 8674.7 | 1296.6 | 1367.0 | 799.9 | 2546.2 | 575.8 |
| ILMN_3242105 | *LOC100134073* | 1118.2 | 1645.1 | 1908.6 | 1344.0 | 2018.4 | 352.7 | 272.7 | 295.4 | 293.0 | 135.0 |
| ILMN_1813131 | *LOC643431* | 1003.5 | 487.1 | 2180.1 | 947.3 | 1268.1 | 256.3 | 245.3 | 320.0 | 252.4 | 165.4 |
| ILMN_1773002 | *LOC730417* | 2074.1 | 1600.1 | 1845.2 | 1127.1 | 680.6 | 494.5 | 389.5 | 320.6 | 418.2 | 264.4 |
| ILMN_1773650 | *LRRN3* | 825.5 | 1664.2 | 1051.0 | 858.6 | 3947.3 | 148.3 | 134.6 | 125.3 | 172.2 | 189.3 |
| ILMN_2048591 | *LRRN3* | 554.8 | 1080.9 | 903.6 | 824.0 | 2438.6 | 123.3 | 131.2 | 124.2 | 151.5 | 125.4 |
| ILMN_2376205 | *LTB* | 1011.7 | 694.1 | 975.9 | 943.5 | 258.8 | 134.0 | 139.3 | 145.0 | 247.3 | 116.1 |
| ILMN_1668863 | *LYPD1* | 2366.7 | 2320.4 | 3759.7 | 2318.7 | 3823.9 | 501.0 | 552.1 | 414.1 | 414.3 | 136.9 |
| ILMN_1679391 | *MAMDC2* | 2275.6 | 7090.7 | 3018.2 | 5091.0 | 11885.4 | 1219.7 | 724.8 | 830.2 | 537.7 | 306.4 |
| ILMN_1711331 | *MAP1LC3C* | 745.3 | 1044.2 | 1240.1 | 693.2 | 912.7 | 232.8 | 164.4 | 159.8 | 188.7 | 183.3 |
| ILMN_1775170 | *MT1X* | 826.1 | 815.0 | 684.4 | 665.2 | 867.2 | 4353.5 | 3349.3 | 7279.1 | 3163.5 | 1727.4 |
| ILMN_1692077 | *MXRA7* | 656.4 | 889.1 | 641.6 | 985.9 | 1003.5 | 134.4 | 122.2 | 143.5 | 164.4 | 466.0 |
| ILMN_1776953 | *MYL9* | 1618.4 | 2350.9 | 1817.3 | 2307.7 | 3461.1 | 263.9 | 242.4 | 322.8 | 304.5 | 1266.6 |
| ILMN_1656111 | *MYLIP* | 304.9 | 396.3 | 310.8 | 238.2 | 634.0 | 1968.8 | 1778.6 | 1898.0 | 1849.8 | 1090.3 |
| ILMN_1713638 | *NIPAL4* | 742.5 | 518.6 | 453.6 | 2005.0 | 617.4 | 125.5 | 133.9 | 126.0 | 129.0 | 130.0 |
| ILMN_1763382 | *NPPB* | 5187.2 | 12750.7 | 7078.6 | 12244.0 | 8760.8 | 133.2 | 127.8 | 137.6 | 220.9 | 138.7 |
| ILMN_1800160 | *NR0B1* | 787.7 | 634.4 | 661.0 | 700.2 | 202.0 | 128.3 | 131.1 | 134.9 | 148.0 | 143.1 |
| ILMN_2094360 | *NR2F2* | 4093.8 | 3408.8 | 5787.4 | 3929.4 | 3501.2 | 110.9 | 130.3 | 121.4 | 131.6 | 1406.4 |
| ILMN_1742025 | *OLFM1* | 383.8 | 558.4 | 234.1 | 371.7 | 276.1 | 1978.4 | 2418.3 | 2517.6 | 1477.4 | 973.3 |
| ILMN_1710544 | *PCDH7* | 948.9 | 2493.0 | 777.4 | 1895.2 | 1940.1 | 152.1 | 148.6 | 168.6 | 308.2 | 242.6 |
| ILMN_1695299 | *PDLIM3* | 1028.5 | 1070.2 | 1135.8 | 1254.5 | 391.7 | 221.9 | 301.5 | 237.2 | 240.2 | 145.8 |
| ILMN_2230025 | *PDLIM3* | 1718.7 | 1416.0 | 1520.2 | 1834.6 | 526.6 | 305.8 | 442.4 | 259.1 | 319.8 | 156.9 |
| ILMN_1690125 | *PDLIM7* | 5842.9 | 6681.6 | 4795.1 | 7360.1 | 4528.1 | 1442.8 | 1312.3 | 1275.8 | 1231.5 | 1995.6 |
| ILMN_2407669 | *PEAR1* | 538.2 | 774.5 | 788.2 | 1320.2 | 624.4 | 121.4 | 121.6 | 124.6 | 138.6 | 469.4 |
| ILMN_1805737 | *PFKP* | 8674.9 | 9485.0 | 10608.3 | 13887.4 | 8011.3 | 3050.3 | 2716.2 | 2441.5 | 2877.2 | 1687.6 |
| ILMN_1671557 | *PHLDA2* | 533.0 | 837.9 | 417.0 | 1027.6 | 518.0 | 144.4 | 134.2 | 138.1 | 159.9 | 251.5 |
| ILMN_1653026 | *PLAC8* | 717.6 | 841.7 | 1492.8 | 3325.0 | 3100.9 | 136.3 | 129.6 | 119.1 | 115.2 | 133.0 |
| ILMN_2093343 | *PLAC8* | 914.9 | 1075.2 | 2724.2 | 4753.7 | 4079.4 | 143.1 | 138.5 | 123.8 | 127.2 | 154.4 |
| ILMN_1656057 | *PLAU* | 11403.7 | 11522.9 | 15488.8 | 18233.0 | 15034.0 | 1123.6 | 960.8 | 960.2 | 645.1 | 1089.4 |
| ILMN_1717706 | *PLK2* | 860.4 | 1025.5 | 1221.5 | 1257.8 | 1509.3 | 170.5 | 165.5 | 174.0 | 164.7 | 215.8 |
| ILMN_1795930 | *PTGER4* | 1641.8 | 2359.4 | 965.1 | 1080.1 | 1434.4 | 182.2 | 184.0 | 188.8 | 179.6 | 202.4 |
| ILMN_1698766 | *PYCARD* | 396.3 | 492.9 | 347.6 | 890.1 | 288.6 | 2455.7 | 2063.6 | 2211.2 | 1855.5 | 1877.0 |
| ILMN_1738558 | *RGS20* | 1353.6 | 2429.1 | 1132.7 | 1936.6 | 3651.0 | 138.9 | 125.3 | 127.6 | 133.7 | 265.6 |
| ILMN_1678215 | *RHOJ* | 548.5 | 640.0 | 436.3 | 1071.6 | 2691.9 | 129.7 | 120.0 | 121.4 | 120.9 | 203.3 |
| ILMN_1722898 | *SFRP2* | 3043.0 | 1758.5 | 2424.4 | 875.0 | 2014.2 | 5639.8 | 5132.9 | 5456.5 | 10523.8 | 8872.8 |
| ILMN_3310065 | *SFTA1P* | 1634.5 | 2337.3 | 1382.5 | 3263.1 | 2306.7 | 142.8 | 137.5 | 139.4 | 124.2 | 136.0 |
| ILMN_1766261 | *SLC2A12* | 928.7 | 1124.5 | 695.5 | 886.8 | 781.8 | 284.2 | 327.0 | 282.5 | 215.9 | 122.5 |

| | | | | | | | | | | | |
|---|---|---|---|---|---|---|---|---|---|---|---|
| ILMN_2407879 | *SORBS2* | 829.9 | 1913.2 | 301.4 | 992.1 | 1696.5 | 168.4 | 170.5 | 188.8 | 167.8 | 184.3 |
| ILMN_1651354 | *SPP1* | 4229.6 | 5784.2 | 6404.3 | 3115.1 | 4009.8 | 303.8 | 381.3 | 806.1 | 402.8 | 169.3 |
| ILMN_2374449 | *SPP1* | 2936.6 | 4594.4 | 3751.1 | 2211.8 | 2791.2 | 238.2 | 235.0 | 665.6 | 304.8 | 170.8 |
| ILMN_2086105 | *SPRY4* | 317.2 | 329.5 | 220.5 | 293.3 | 195.7 | 2965.1 | 3106.1 | 2462.8 | 3533.8 | 494.8 |
| ILMN_1667460 | *SULF2* | 2099.8 | 1850.7 | 3194.4 | 2147.2 | 1709.4 | 489.5 | 504.9 | 453.7 | 414.8 | 1226.8 |
| ILMN_1686981 | *SULF2* | 680.3 | 676.6 | 953.8 | 916.3 | 935.4 | 155.4 | 156.4 | 139.2 | 156.9 | 538.0 |
| ILMN_2345142 | *SULF2* | 1326.7 | 1478.3 | 1616.6 | 1525.0 | 1872.5 | 338.0 | 258.5 | 265.0 | 240.4 | 852.4 |
| ILMN_2400935 | *TAGLN* | 8903.3 | 13503.2 | 8369.1 | 13263.2 | 12888.8 | 1049.9 | 641.6 | 1113.6 | 1025.8 | 4064.0 |
| ILMN_1662619 | *TFPI* | 1359.5 | 2360.4 | 1552.8 | 1614.8 | 5130.7 | 150.7 | 131.4 | 159.2 | 277.7 | 716.3 |
| ILMN_1812526 | *TGFB2* | 340.4 | 1096.8 | 472.3 | 834.1 | 2695.1 | 118.1 | 113.8 | 118.2 | 112.9 | 115.2 |
| ILMN_1679267 | *TGM2* | 458.8 | 668.9 | 736.6 | 1090.2 | 768.0 | 157.6 | 155.4 | 127.4 | 144.5 | 247.0 |
| ILMN_1705750 | *TGM2* | 3031.6 | 3621.6 | 6073.6 | 15707.0 | 10241.9 | 160.2 | 181.2 | 147.5 | 178.8 | 751.6 |
| ILMN_1804663 | *THBS3* | 2661.0 | 2209.7 | 3625.5 | 2587.5 | 1815.5 | 233.6 | 266.3 | 287.2 | 252.5 | 1294.8 |
| ILMN_1736078 | *THBS4* | 320.4 | 165.8 | 214.7 | 252.7 | 135.3 | 879.2 | 843.6 | 799.2 | 499.1 | 944.4 |
| ILMN_1779875 | *THY1* | 1079.1 | 1636.7 | 1273.6 | 2810.6 | 1118.2 | 6743.1 | 7021.1 | 6430.4 | 6884.4 | 12613.6 |
| ILMN_1770338 | *TM4SF1* | 3151.1 | 2595.4 | 1442.7 | 4095.7 | 4456.1 | 142.9 | 128.8 | 133.5 | 186.2 | 342.4 |
| ILMN_1678403 | *TMEM178* | 730.2 | 1266.0 | 546.8 | 759.4 | 927.8 | 253.3 | 215.2 | 371.5 | 256.6 | 115.3 |
| ILMN_1757129 | *TMEM88* | 1544.3 | 1689.2 | 1978.5 | 2553.6 | 910.3 | 282.7 | 209.8 | 160.4 | 250.0 | 120.5 |
| ILMN_1699695 | *TNFRSF21* | 10778.0 | 11540.3 | 12188.4 | 13621.3 | 6880.1 | 3061.5 | 3023.0 | 2998.7 | 3452.4 | 967.6 |
| ILMN_2331231 | *TNFRSF6B* | 415.9 | 468.2 | 575.9 | 1374.4 | 550.4 | 139.8 | 139.8 | 135.4 | 149.1 | 299.4 |
| ILMN_1699489 | *TUBB6* | 5562.1 | 5894.3 | 5388.3 | 7773.9 | 5195.4 | 1156.7 | 1166.1 | 1236.3 | 836.2 | 3929.7 |
| ILMN_1702636 | *TUBB6* | 2811.8 | 4374.7 | 2407.1 | 3746.3 | 4410.1 | 511.0 | 459.3 | 687.2 | 437.2 | 2125.2 |
| ILMN_1678841 | *UBD* | 923.8 | 1281.3 | 344.6 | 729.5 | 690.4 | 121.8 | 136.4 | 141.3 | 131.4 | 150.9 |
| ILMN_1671969 | *UGP2* | 276.4 | 321.0 | 283.1 | 150.9 | 447.3 | 1444.6 | 1587.7 | 1824.9 | 2311.1 | 815.9 |
| ILMN_2389155 | *UGP2* | 520.8 | 574.3 | 574.4 | 509.8 | 933.7 | 3017.8 | 3415.4 | 2686.0 | 3646.7 | 1546.0 |
| ILMN_2307903 | *VCAM1* | 1023.4 | 498.9 | 577.8 | 598.4 | 286.0 | 118.0 | 100.7 | 120.4 | 122.6 | 258.2 |
| ILMN_1760315 | *VWCE* | 1247.7 | 1776.0 | 1025.5 | 1601.5 | 564.3 | 269.3 | 361.8 | 342.8 | 179.4 | 231.3 |
| ILMN_1740269 | *WNT2B* | 1943.1 | 1711.3 | 981.8 | 1639.9 | 1088.8 | 121.8 | 120.1 | 124.0 | 115.9 | 225.2 |
| ILMN_1779015 | *ZNF467* | 810.0 | 422.2 | 968.5 | 587.3 | 357.5 | 119.4 | 137.1 | 122.1 | 209.0 | 182.0 |